



Intensity effects of light coupling to one- or two-atom arrays of infinite extentF. Robicheaux ^{1,2,*} and Deepak A. Suresh ¹¹*Department of Physics and Astronomy, Purdue University, West Lafayette, Indiana 47907, USA*²*Purdue Quantum Science and Engineering Institute, Purdue University, West Lafayette, Indiana 47907, USA*

(Received 17 April 2023; accepted 14 July 2023; published 26 July 2023)

We theoretically and computationally investigate the behavior of infinite atom arrays when illuminated by nearly resonant light. We use higher-order mean-field equations to investigate the coherent reflection and transmission and incoherent scattering of photons from a single array and from a pair of arrays as a function of detuning for different values of the Rabi frequency. For the single array case, we show how increasing the light intensity changes the probabilities for these different processes. For example, the incoherent scattering probability initially increases with light intensity before decreasing at higher values. For a pair of parallel arrays at near resonant separation, the effects from increasing light intensity can become apparent with incredibly low-intensity light. In addition, we derive the higher-order mean-field equations for these infinite arrays, giving a representation that can be evaluated with a finite number of equations.

DOI: [10.1103/PhysRevA.108.013711](https://doi.org/10.1103/PhysRevA.108.013711)**I. INTRODUCTION**

Interesting many-body effects occur when light interacts with many atoms with separations less than the light's wavelength. In this case, a photon coherently interacts with many atoms, leading to collective effects that can be difficult to anticipate from single atom-photon interactions. There are several interesting scenarios when the atoms are in a regular array [1–36] because the dephasing that occurs due to the dipole-dipole interaction is reduced and photon interference from different emitters can lead to qualitatively new phenomena. One fascinating scenario involves the manipulation of light using atom arrays [3–8,17–29] by modifying transmission, reflection, scattering, and diffraction.

Most previous studies have investigated atomic arrays with much less than one excitation on average; the exceptions we have noted are in Refs. [14–16,18–20,27,29,31–36]. This limit holds when very weak light interacts with atoms initially in the ground state. We denote this limit of very weak light as the weak-field approximation (WFA). In this limit, the atoms can be treated as harmonic oscillators instead of two-level systems, which means most results are indistinguishable from the interaction of light with classical oscillators. Although classical electromagnetism explains most of these results, several groups have proposed or measured quite interesting phenomena. At the other limit of computational complexity are calculations that utilize the full density matrix as in Refs. [14–16,18,19,29,31,33,34]. For many systems, a mean-field approximation would lead to sufficiently accurate results for most combinations of parameters [20].

In this paper, we present the results of our investigation of the interaction of light, beyond the WFA, with one or two infinite arrays of atoms. We focus on two aspects of this system.

The first is to develop a method that accurately represents the physics with only a finite number of equations. This is not a trivial undertaking because there are an infinite number of density matrix elements for more than one excitation. Even weak light leads to an infinite number of excitations, although only a finite fraction of the atoms are excited. To model this system, we extended the higher-order mean-field theory in Ref. [37] to use a mixed-order method for the infinite array. The main idea is to have pairwise expectation values $\langle \hat{A}_n \hat{B}_m \rangle$ for atoms n and m smoothly transition to products $\langle \hat{A}_n \rangle \langle \hat{B}_m \rangle$ as the atom separation increases. The second is to explore the trends for the coherent reflection or transmission from the array(s) as well as the incoherent scattering. In this, we somewhat overlap with previous results in Ref. [20] for a single array.

All of the cases treated here have the atoms perfectly placed on an infinite lattice and the recoil of the atoms is neglected. For simplicity, all examples are for a square lattice with the plane-wave light incident perpendicular to the arrays. The details of some phenomena depend on these specific conditions (for example, the reflection or transmission of light not normally incident on the array), but there does not appear to be qualitative changes. Although perfect, uniformly illuminated, infinite arrays are not experimentally accessible, the simplifications that result from this ideal case could aid in interpreting results from finite, imperfect arrays. For one array, we explored the coherent reflection and transmission and the incoherent scattering of the photons as a function of detuning and intensity. As an example, we showed how the 100% coherent reflection on resonance in the WFA changes to incoherent scattering and some transmission as the intensity increases. As another example, we found that the lowest-order mean-field approximation overestimates the incoherent scattering probability by 15% in the limit of very low intensity. For two arrays, we found that the effects beyond the WFA can be present at very small incident intensity.

*robichf@purdue.edu

II. BASIC THEORY

In all that follows, we will assume the atoms couple to the light through a closed two-level transition. Also, the atoms will be driven by a classical plane wave normally incident on the atom arrays to simplify some of the derivations. For the n th atom, the ground and excited states are $|g_n\rangle$ and $|e_n\rangle$. The operators used below follow the definition

$$\hat{e}_n \equiv |e_n\rangle\langle e_n| \quad \hat{\sigma}_n^- \equiv |g_n\rangle\langle e_n| \quad \hat{\sigma}_n^+ \equiv |e_n\rangle\langle g_n|. \quad (1)$$

The position of the n th atom is \mathbf{R}_n .

The basic theory is identical to that in Ref. [37], where the density matrix equations are converted into equations of motion of the expectation values of operators. It also uses cumulants, Ref. [38], to reduce expectation values of products of operators into products of lower-order expectation values as done in Refs. [1,14,35,36,39–46]. We will call the replacement of pairwise expectation values by the product of the expectation value (e.g., $\langle \hat{A}\hat{B} \rangle \rightarrow \langle \hat{A} \rangle \langle \hat{B} \rangle$) the mean-field or mean-field-1 (MF1) approximation. We will call the replacement of triple expectation values by products of pairwise and single expectation values the mean-field-2 (MF2) approximation (e.g., $\langle \hat{A}\hat{B}\hat{C} \rangle \rightarrow \langle \hat{A}\hat{B} \rangle \langle \hat{C} \rangle + \langle \hat{A} \rangle \langle \hat{B}\hat{C} \rangle + \langle \hat{B} \rangle \langle \hat{A}\hat{C} \rangle - 2\langle \hat{A} \rangle \langle \hat{B} \rangle \langle \hat{C} \rangle$). The WFA is obtained when all operator products and all $\langle \hat{e} \rangle$ are set to zero.

The coupling between atom pairs through the quantized electromagnetic field is through the dyadic Green's function. For $m \neq n$, we will define

$$g_{mn} = g(\mathbf{R}_m - \mathbf{R}_n) \quad (2)$$

$$g(\mathbf{R}) = \frac{\Gamma}{2} \left[h_0^{(1)}(s) + \frac{3\hat{R} \cdot \hat{d}^* \hat{R} \cdot \hat{d} - 1}{2} h_2^{(1)}(s) \right], \quad (3)$$

with \hat{d} the dipole unit vector, $s = kR$, $\hat{R} = \mathbf{R}/R$, and $h_\ell^{(1)}(s)$ the outgoing spherical Hankel function of angular momentum ℓ : $h_0^{(1)}(s) = e^{is}/[is]$ and $h_2^{(1)}(s) = (-3i/s^3 - 3/s^2 + i/s)e^{is}$. The $g(\mathbf{R})$ is proportional to the propagator that gives the electric field at \mathbf{R} given a dipole at the origin [47]. For a $\Delta M = 0$ transition, $\hat{d} = \hat{z}$ and the coefficient of the $h_2^{(1)}$ Bessel function is $P_2[\cos(\theta)] = [3\cos^2(\theta) - 1]/2$, where $\cos(\theta) = Z/R$. For a $\Delta M = \pm 1$ transition, the coefficient of the $h_2^{(1)}$ Bessel function is $-(1/2)P_2[\cos(\theta)] = [1 - 3\cos^2(\theta)]/4$.

For simplicity, the atoms will be on a square array with separation a . We will have the atoms at the position $\mathbf{R}_n = (x_0, n_y a, n_z a)$, where $x_0 = 0$ for the single-array calculations and $x_0 = 0$ or L for the two-array calculations.

Some simplifications to one- and two-atom expectation values occur due to Bloch's theorem when the light is normally incident on the array. The first is that the one-atom expectation values are independent of position in that array. For example, for the single array calculations, we will use

$$\langle \hat{e}_n \rangle = \langle \hat{e}_0 \rangle \equiv \langle \hat{e} \rangle \quad \text{and} \quad \langle \hat{\sigma}_n^\pm \rangle = \langle \hat{\sigma}_0^\pm \rangle \equiv \langle \hat{\sigma}^\pm \rangle. \quad (4)$$

The other is that two-atom expectation values can be shifted so that one operator is at the origin for that array. For example, for the single-array calculations, we will use

$$\langle \hat{A}_{n_y, n_z} \hat{B}_{m_y, m_z} \rangle = \langle \hat{A}_0 \hat{B}_{m_y - n_y, m_z - n_z} \rangle \quad (5)$$

or the index 0 for the \hat{B} and the index $n_y - m_y, n_z - m_z$ for the \hat{A} .

The equations of motion for single-atom operators ignoring the interaction between atoms are

$$\begin{aligned} \frac{d\langle \hat{\sigma}^- \rangle}{dt} &= \left[i\Delta - \frac{\Gamma}{2} \right] \langle \hat{\sigma}^- \rangle + i\frac{\Omega}{2} (2\langle \hat{e} \rangle - 1) \\ \frac{d\langle \hat{e} \rangle}{dt} &= -\Gamma \langle \hat{e} \rangle + i\frac{\Omega^*}{2} \langle \hat{\sigma}^- \rangle - i\frac{\Omega}{2} \langle \hat{\sigma}^+ \rangle, \end{aligned} \quad (6)$$

where the equation for $\langle \hat{\sigma}^+ \rangle$ is the complex conjugate of the first. When finding the equations for products of operators, use these equations with the product rule for derivatives.

III. MF1 EQUATIONS OF MOTION

In the time-dependent equations for the $\langle \hat{e} \rangle$ and $\langle \hat{\sigma}^\pm \rangle$ expectation values, only the 0 index terms contribute as discussed above. The MF1 approximation leads to the replacement of pairwise expectation values: $\langle \hat{A}_n \hat{B}_m \rangle \rightarrow \langle \hat{A}_n \rangle \langle \hat{B}_m \rangle \rightarrow \langle \hat{A}_0 \rangle \langle \hat{B}_0 \rangle \equiv \langle \hat{A} \rangle \langle \hat{B} \rangle$, see Eq. (4).

A. One array

The differential equations for the one-atom expectation values have one-atom terms from the interaction with the laser and the single-photon decays in the Lindbladian as well as two-atom terms, Eq. (A1), from the dipole-dipole interactions. The two-atom terms in Eq. (A1) become independent of m for MF1 and the sum over all atoms $m \neq 0$ leads to the definition

$$\mathcal{G} \equiv \sum_{m \neq 0} g(\mathbf{R}_m) \equiv i\delta + \frac{\gamma}{2}, \quad (7)$$

where Ref. [7] showed $\gamma/\Gamma = (3/[4\pi])(\lambda/a)^2 - 1$. We discuss the numerical evaluation of \mathcal{G} in Appendix C. The equations of motion are

$$\begin{aligned} \frac{d\langle \hat{\sigma}^- \rangle}{dt} &= \left[i\Delta - \frac{\Gamma}{2} \right] \langle \hat{\sigma}^- \rangle + i\frac{\bar{\Omega}}{2} (2\langle \hat{e} \rangle - 1) \\ \frac{d\langle \hat{e} \rangle}{dt} &= -\Gamma \langle \hat{e} \rangle + i\frac{\bar{\Omega}^*}{2} \langle \hat{\sigma}^- \rangle - i\frac{\bar{\Omega}}{2} \langle \hat{\sigma}^+ \rangle, \end{aligned} \quad (8)$$

where $\bar{\Omega} = \Omega - 2i\mathcal{G}\langle \hat{\sigma}^- \rangle$ and the equation for $\langle \hat{\sigma}^+ \rangle$ is the complex conjugate of the first. The $\bar{\Omega}$ can be thought of as the total field from the laser plus that from all other dipoles. The steady-state values can be found by setting the left-hand side equal to zero with the solution being found using Newton's iterative method.

The coherent reflection (R), coherent transmission (T), and incoherent scattering (S) probability of light can be determined from derivations in Appendix B. For the coherent reflection and transmission probabilities, Eq. (B8) gives the far-field form of the electric field from which

$$\mathbf{R} = |\mathcal{R}|^2 \quad \text{and} \quad \mathbf{T} = |1 + \mathcal{R}|^2, \quad (9)$$

$$\mathcal{R} = -\frac{3i\Gamma\pi}{\Omega k^2 a^2} \langle \hat{\sigma}^- \rangle, \quad (10)$$

with \mathcal{R} derived in Eq. (B9). The incoherent scattering is given by Eq. (B13) because $Q^{(2)} = 0$ at the MF1 level:

$$\mathbf{S} = 2 \times 3\pi \left(\frac{\Gamma}{\Omega k a} \right)^2 [\langle \hat{\epsilon} \rangle - |\langle \hat{\sigma}^+ \rangle|^2], \quad (11)$$

where the factor of 2 accounts for scattering in both the $\pm x$ directions.

B. Two arrays

For this case, we will designate the array at $x = 0$ to be α and that at $x = L$ to be β . The expectation values of the operators in each array can be different so we need to distinguish the array with a subscript, for example, $\langle \hat{\epsilon}_\alpha \rangle$. There is a new constant due to the interaction between the two arrays:

$$\bar{\mathcal{G}} \equiv e^{-ikL} \sum_{m_\beta} g(\mathbf{R}_{m_\beta}), \quad (12)$$

where the m_β means to sum over all of the atoms in the array at $x = L$ and the \mathbf{R}_{m_β} are the positions measured relative to the 0 atom in array α . We have defined $\bar{\mathcal{G}}$ with a factor of $\exp(-ikL)$ so that the main dependence on array separation is visible in the equations of motion. We discuss the numerical evaluation of $\bar{\mathcal{G}}$ in Appendix C. If L is larger than a few λ , the sum is, to an excellent approximation, $\bar{\mathcal{G}} = (3\pi/2)\Gamma/(ka)^2$, see Appendix C. The equations of motion are

$$\begin{aligned} \frac{d\langle \hat{\sigma}_\alpha^- \rangle}{dt} &= \left[i\Delta - \frac{\Gamma}{2} \right] \langle \hat{\sigma}_\alpha^- \rangle + i\frac{\bar{\Omega}_\alpha}{2} (2\langle \hat{\epsilon}_\alpha \rangle - 1) \\ \frac{d\langle \hat{\epsilon}_\alpha \rangle}{dt} &= -\Gamma \langle \hat{\epsilon}_\alpha \rangle + i\frac{\bar{\Omega}_\alpha^*}{2} \langle \hat{\sigma}_\alpha^- \rangle - i\frac{\bar{\Omega}_\alpha}{2} \langle \hat{\sigma}_\alpha^+ \rangle \\ \frac{d\langle \hat{\sigma}_\beta^- \rangle}{dt} &= \left[i\Delta - \frac{\Gamma}{2} \right] \langle \hat{\sigma}_\beta^- \rangle + i\frac{\bar{\Omega}_\beta}{2} (2\langle \hat{\epsilon}_\beta \rangle - 1) \\ \frac{d\langle \hat{\epsilon}_\beta \rangle}{dt} &= -\Gamma \langle \hat{\epsilon}_\beta \rangle + i\frac{\bar{\Omega}_\beta^*}{2} \langle \hat{\sigma}_\beta^- \rangle - i\frac{\bar{\Omega}_\beta}{2} \langle \hat{\sigma}_\beta^+ \rangle, \end{aligned} \quad (13)$$

where the effective field at array α is $\bar{\Omega}_\alpha = \Omega - 2i(\bar{\mathcal{G}}\langle \hat{\sigma}_\alpha^- \rangle + \bar{\mathcal{G}}e^{ikL}\langle \hat{\sigma}_\beta^- \rangle)$ and at array β is $\bar{\Omega}_\beta = \Omega e^{ikL} - 2i(\bar{\mathcal{G}}\langle \hat{\sigma}_\beta^- \rangle + \bar{\mathcal{G}}e^{ikL}\langle \hat{\sigma}_\alpha^- \rangle)$. The coupling between the two arrays is through the $\bar{\Omega}$ parameters.

As with the previous section, the coherent reflection, coherent transmission, and incoherent scattering probability can be determined from derivations in Appendix B. For the coherent reflection and transmission probabilities, Eq. (B11) gives the far-field form of the electric field from which

$$\mathbf{R} = |\mathcal{R}_\alpha + \mathcal{R}_\beta e^{ikL}|^2, \quad (14)$$

$$\mathbf{T} = |1 + \mathcal{R}_\alpha + \mathcal{R}_\beta e^{-ikL}|^2, \quad (15)$$

with \mathcal{R} given in Eq. (10) with the expectation value of the appropriate array. As with the previous section, the incoherent scattering is given by Eq. (B13) because $Q^{(2)} = 0$ at the MF1 level:

$$\mathbf{S} = 2 \times 3\pi \left(\frac{\Gamma}{\Omega k a} \right)^2 [\langle \hat{\epsilon}_\alpha \rangle - |\langle \hat{\sigma}_\alpha^+ \rangle|^2 + \langle \hat{\epsilon}_\beta \rangle - |\langle \hat{\sigma}_\beta^+ \rangle|^2], \quad (16)$$

where the factor of 2 accounts for scattering in both $\pm x$ directions.

An interesting parameter is the buildup of coherent light between the arrays. When the position is not too close to the arrays, the coherent electric field between the arrays is

$$\vec{E} = \hat{\epsilon} [(1 + \mathcal{R}_\alpha)e^{ikx} + \mathcal{R}_\beta e^{ikL}e^{-ikx}], \quad (17)$$

where $\hat{\epsilon}$ is the polarization. The scaled, average intensity between the arrays can be found by taking the magnitude squared and averaging between 0 and L , giving

$$\langle I \rangle / I_{\text{inc}} = |1 + \mathcal{R}_\alpha|^2 + |\mathcal{R}_\beta|^2 \quad (18)$$

when the distance between the arrays is nearly an integer number of wavelengths.

IV. MF2 EQUATIONS OF MOTION

In the MF2 approximation, the differential equations for the single-atom expectation values do not directly contain an approximation. The differential equations for two-atom expectation values have terms that arise from the one-atom terms in the Hamiltonian (from the laser) and the Lindbladian (from the single-atom decays) which, because they only contain pair expectation values, do not have approximations. The terms that arise from the dipole-dipole interactions have two- and three-atom expectation values. The three-atom terms are approximated as two- and one-atom expectation values as discussed in Appendix A.

The only important two-atom terms arising from the dipole-dipole interactions are

$$\frac{d\langle \hat{\epsilon}_0 \hat{\sigma}_n^- \rangle}{dt} = -g_{n0}^* \langle \hat{\epsilon}_n \hat{\sigma}_0^- \rangle - V_1 - V_2 + 2V_3 - V_4 \quad (19)$$

$$\frac{d\langle \hat{\sigma}_0^- \hat{\sigma}_n^- \rangle}{dt} = 2V_5 - V_6 + 2V_7 - V_8 \quad (20)$$

$$\frac{d\langle \hat{\epsilon}_0 \hat{\epsilon}_n \rangle}{dt} = -V_9 - V_{10} - V_{11} - V_{12} \quad (21)$$

$$\begin{aligned} \frac{d\langle \hat{\sigma}_0^- \hat{\sigma}_n^+ \rangle}{dt} &= (g_{n0} + g_{n0}^*) (2\langle \hat{\epsilon}_0 \hat{\epsilon}_n \rangle - \langle \hat{\epsilon}_0 \rangle) \\ &\quad + 2V_{13} - V_{14} + 2V_{15} - V_{16} \end{aligned} \quad (22)$$

with the definitions and derivations in Appendix A. All other expectation values can be derived from these. Including the equations of motion from the single-atom operators, use Eq. (6) with the product rule for derivatives. For example, the contribution to the equation for $\langle \hat{\epsilon}_0 \hat{\epsilon}_n \rangle$ is

$$\begin{aligned} \frac{d\langle \hat{\epsilon}_0 \hat{\epsilon}_n \rangle}{dt} &= -2\Gamma \langle \hat{\epsilon}_0 \hat{\epsilon}_n \rangle + i\frac{\Omega^*}{2} (\langle \hat{\sigma}_0^- \hat{\epsilon}_n \rangle + \langle \hat{\epsilon}_0 \hat{\sigma}_n^- \rangle) \\ &\quad - i\frac{\Omega}{2} (\langle \hat{\sigma}_0^+ \hat{\epsilon}_n \rangle + \langle \hat{\epsilon}_0 \hat{\sigma}_n^+ \rangle). \end{aligned} \quad (23)$$

For the MF2 equations, we have not derived the equations for two arrays. The results for one array changed by at most 10%–20%, going from MF1 to MF2 for some values of detuning and Rabi frequency. Going from one to two arrays will lead to twice as many single-atom expectation values and $4\times$ as many pair expectation values. In addition, there will be at least $8\times$ the required CPU time. We estimated that the computer requirements were somewhat beyond our local resources and, therefore, did not attempt an MF2 calculation for two arrays.

V. RESULTS

In this section, we present the results of calculations for light incident on one- or two-atom arrays. We are specifically interested in how the light intensity changes the results from that in the weak-field limit.

A. One infinite array: R, T, S

In this section, we consider the coherent reflection (R), coherent transmission (T), and incoherent scattering (S) of plane-wave light normally incident on a single-layer atom array. The atoms will be on a square array with separation $a < \lambda$ and approximated as a two-level system. Reference [4] predicted the total reflection of light for the correct detuning from a perfect, single-layer atomic array, and this system was further explored in Ref. [7]. Substantial reflection was experimentally measured from a single-layer atom array [24]. The calculations [4,7] were in the weak-laser limit where multiple atom excitations are ignored. A key question is how well does the weak-laser approximation work as a function of intensity and how does the weak-laser approximation fail with increasing intensity? Reference [20] presented some results for a Gaussian beam incident on a 10×10 array for incident intensity up to $100 I_{\text{sat}}$ (see their Fig. 6). They addressed similar physics questions to those in this section using (what we call) the MF1 approximation and found similar results.

It seems clear that the amount of reflection will degrade as the intensity increases. At low intensity, the atoms can be approximated as harmonic oscillators, which is assumed in Refs. [4,7]. The two-state character of the atoms becomes increasingly important as the Rabi frequency approaches Γ . To investigate the role of intensity, we performed MF1 and MF2 calculations of light on a perfect, square array with separation $a = 0.8 \lambda$. Calculations with separation 0.4 and 0.6λ gave similar results. In both MF1 and MF2 calculations, we solved the time-dependent equations until the solutions reached a steady state. The calculations were done with laser intensities $2 \times 10^{-8}, 2 \times 10^{-7}, 2 \times 10^{-6}, \dots, 20, 200 I_{\text{sat}}$. The Rabi frequency is $\Omega = \Gamma \sqrt{0.5I/I_{\text{sat}}}$ giving $10^{-4}, \sqrt{10} \times 10^{-4}, 10^{-3}, \dots, \sqrt{10}, 10 \Gamma$.

Figure 1 shows the transmitted, reflected, and scattered probabilities versus detuning for different intensities. We only show the MF1 calculations where there is a clear difference from that for MF2. Even when there is a clear difference, the difference is not large. On resonance, there is a larger proportion of photons transmitted or scattered and a smaller proportion reflected as the laser intensity increases. This trend is not surprising. Even for these somewhat larger intensities, up to $I = 0.2 I_{\text{sat}}$, the effect of intensity is larger for reflection than transmission; for example, the green dash curve (MF2, $I = 0.02 I_{\text{sat}}$, $\Omega = 0.1 \Gamma$) has approximately 34% of the photons scattered, 5% transmitted, and 61% reflected. That is, there is still only a few coherently transmitted photons, so most of the photons not reflected are scattered. This figure indicates that the laser intensity needs to be less than $\sim 0.002 I_{\text{sat}}$, $\Omega \sim 0.03 \Gamma$, to keep the fraction of scattered photons less than $\sim 10\%$. These values depend on the spacing of the lattice. For $a = 0.6 \lambda$, there is $\sim 5 \times$ less scattering for low intensity but becomes similar at higher intensity. For

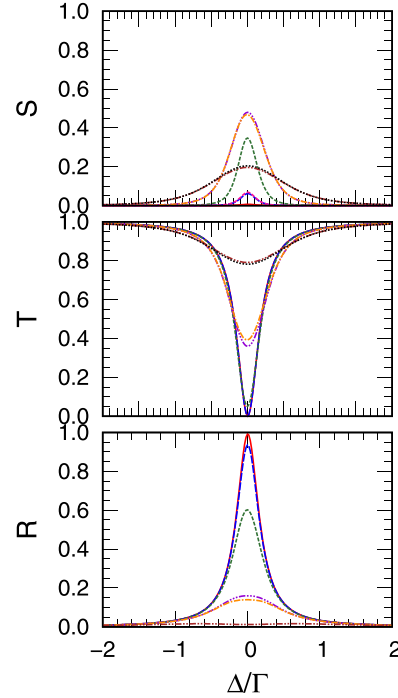


FIG. 1. The coherently reflected (R), coherently transmitted (T), and incoherently scattered (S) probabilities versus detuning Δ for different intensities and approximation levels. The intensity is stepped by powers of 10 and given in terms of the saturation intensity: $I/I_{\text{sat}} = 2\Omega^2/\Gamma^2$. The MF2 calculations are red solid (2×10^{-4}), blue long dash (2×10^{-3}), green dash (0.02), orange dash-dot (0.2), and maroon dash-dot-dot (2). In all plots, the purple long dash is for MF1 with intensity 0.2. In the T and S plots, the black dot is for MF1 with intensity 2. In the S plot, the pink dash is for MF1 with intensity 2×10^{-3} .

example, at $0.002 I_{\text{sat}}$, there is $\simeq 6\%$ ($\simeq 1.2\%$) scattering for 0.8λ (0.6λ), while at $0.2 I_{\text{sat}}$ both have a peak scattering of $\sim 40\%$.

As the laser intensity increases from small values, the fraction of incoherently scattered photons is proportional to the laser intensity times the square of the reflection probability. Thus, the *fraction* of photons that are incoherently scattered goes to zero as the laser intensity is decreased. For weak laser intensity, there is little change to the transmitted probability; the largest change as the intensity increases is a decrease in the coherent reflected probability. For example, at $\Delta = 0$ for MF2, there is 6.2% incoherently scattered photons, 93.7% reflected, and 0.1% transmitted for $I = 0.002 I_{\text{sat}}$ (i.e., $\Omega \simeq 0.032 \Gamma$), while there was 0.67% scattered and 99.3% reflected for $10 \times$ smaller intensity (i.e., $\Omega = 0.01 \Gamma$). It is interesting that the MF1 and MF2 incoherently scattered probability has a ratio at the peak that is independent of the laser intensity for small intensity: $S(\text{MF1})/S(\text{MF2}) = 1.15$ as $I \rightarrow 0$. This is a surprising result because one might expect that MF1 becomes a better approximation as the fraction of atoms excited is decreased. While this is correct for reflection and transmission probabilities, it is not correct for incoherent scattering because the scattered probability depends on two-atom correlations.

As expected, the resonance width increases as the intensity increases. For smaller intensity, this is more due to increased decoherence due to incoherent scattering than to power broadening. For larger intensity, power broadening becomes increasingly relevant.

Interestingly, as the intensity continues to increase, the fraction of photons on resonance that are scattered starts to decrease. This is mainly due to the rate of incoming photons becoming larger than the rate they can be incoherently scattered. Also, as expected, the fraction of photons reflected becomes quite small while the fraction transmitted increases toward 1 as the intensity increases.

B. Two parallel arrays

Two parallel arrays can act as a cavity. This can lead to large intensity between the arrays, which can affect the reflection, transmission, and incoherent scattering properties at much smaller incident intensities. As an example, Ref. [17] investigated several aspects of weak light interacting with two-dimensional atomic lattices, starting with a pair of lattices and going to stacks of lattices. All of the calculations in this section use MF1 with the arrays separated by 5.01λ and the atom separation within an array $a = 0.8\lambda$. The cavity enhancement of intensity between the array and the narrowness of the resonance depends on how close the separation is to an integer (or half-integer) number of wavelengths; the value 5.01λ was chosen to give a cavity enhancement of a few 100 on resonance. From the previous section, there is approximately 15% more incoherently scattered light when using the MF1 approximation compared to MF2 for one array. Therefore, the intensity effects will be somewhat exaggerated in these calculations but the approximate sizes and the trends should be correct.

We first derive the expected result in the weak-field approximation when the array separation is much larger than the atom spacing within one array, $L \gg a$. In this limit, the scattering from each array can be done self-consistently using the notation of Appendix B:

$$\mathcal{R} = -\frac{3i\Gamma\pi}{\Omega k^2 a^2} \frac{\Omega/2}{\Delta + i(\Gamma/2) + i\mathcal{G}}$$

$$\langle \eta_E^+ \rangle(x < L) = \hat{\varepsilon}(e^{ikx} + \mathcal{R}e^{ik|x|} + A_\alpha[e^{-ikx} + \mathcal{R}e^{ik|x|}])$$

$$\langle \eta_E^+ \rangle(x > 0) = \hat{\varepsilon}A_\beta(e^{ik(x-L)} + \mathcal{R}e^{ik|x-L|}) \quad (24)$$

where we used the weak-field approximation to calculate \mathcal{R} and used the fact that the reflection amplitude is the same for both left- and right-going waves. The two coefficients, $A_{\alpha,\beta}$, are determined by making the two expressions equal in the region $0 < x < L$. This leads to the two equations $1 + \mathcal{R} + \mathcal{R}A_\alpha = A_\beta e^{-ikL}$ and $A_\alpha = A_\beta \mathcal{R}e^{ikL}$ giving

$$A_\alpha = \frac{\mathcal{R}(1 + \mathcal{R})}{1 - \mathcal{R}^2 e^{2ikL}} e^{2ikL} \quad (25)$$

$$A_\beta = \frac{1 + \mathcal{R}}{1 - \mathcal{R}^2 e^{2ikL}} e^{ikL}. \quad (26)$$

The total reflection and transmission amplitudes are

$$\mathcal{R}_{\text{tot}} = \mathcal{R} + (1 + \mathcal{R})A_\alpha$$

$$\mathcal{T}_{\text{tot}} = (1 + \mathcal{R})A_\beta e^{-ikL} \quad (27)$$

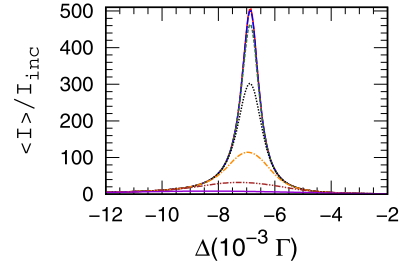


FIG. 2. The relative average intensity between the arrays versus detuning for several incident intensities (in terms of I_{sat}): red solid (weak-field approximation), blue dashed (2×10^{-9}), green short dash (2×10^{-8}), black dotted (2×10^{-7}), orange dash-dot (2×10^{-6}), maroon dash-dot-dot (2×10^{-5}), and purple dash-dot-dot-dot (2×10^{-4}). The arrays are separated by 5.01λ and the atom separation $a = 0.8\lambda$.

The relative average of the intensity between the arrays (average intensity between the arrays divided by incident intensity) can be found using $\langle \eta_E^+ \rangle(x > 0)$ by taking the magnitude squared and averaging between 0 to L , giving

$$\langle I \rangle / I_{\text{inc}} = |A_\beta|^2 (1 + |\mathcal{R}|^2) \quad (28)$$

in the weak-field limit.

As with all cavities, the largest response is when the reflection probability is close to 1, which implies array separations close to an integer number of wavelengths. This will lead to a transmission probability with a narrow resonance and a sharp peak in the average intensity between the arrays. The increased intensity between the arrays leads to a conflict for the response of the array pair. The peak intensity between the arrays increases with the narrowness of the line. But as the incident intensity I_{inc} increases, there will be more incoherent scattering from the effects discussed in Sec. V A, which will lead to a broadening of the line and a decrease in relative intensity between the arrays.

This can be seen in Fig. 2, where the average intensity between the arrays divided by the incident intensity is plotted versus detuning for the weak-field approximation and several incident intensities, from 2×10^{-9} to $2 \times 10^{-4} I_{\text{sat}}$. The results approach that for the weak-field approximation as the incident intensity decreases. As expected, the relative intensity between the arrays decreases with increasing incident intensity. The surprising aspect might be at how small an intensity the decrease becomes noticeable. At $2 \times 10^{-8} I_{\text{sat}}$ incident intensity, the peak value is decreased by approximately 8.3% from the weak-field limit. This is approximately the same factor of incoherently scattered photons. In fact, for low intensities, the relative difference in the intensity from the weak-field approximation approximately equals the fraction of photons scattered for detunings in the neighborhood of the resonance. From Sec. V A, approximately 10% scattering occurred for $2 \times 10^{-3} I_{\text{sat}}$. Making a crude estimate that the intensity is $500\times$ larger and there are two arrays, one might expect an effective intensity $1000\times$ larger than $2 \times 10^{-8} I_{\text{sat}}$, giving an effective intensity for incoherent scattering of $2 \times 10^{-5} I_{\text{sat}}$. For the two arrays, we expected an incoherently scattered probability closer to 0.083%. Thus, the incoherent

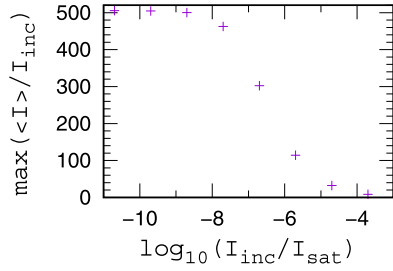


FIG. 3. The peak relative average intensity between the arrays versus the incident intensity.

scattering for two arrays could be much larger than from simple estimates.

Figure 3 shows the peak of the relative average intensity between the arrays plotted versus the incident intensity for intensities from 2×10^{-11} to $2 \times 10^{-4} I_{\text{sat}}$. At low intensities, it goes to the value for the weak-field approximation, ~ 500 . At $2 \times 10^{-4} I_{\text{sat}}$, it has decreased by a factor of ~ 60 to ~ 8 , which is still a large enhancement.

Changing the array separation to 5.01414λ (i.e., increase the displacement from integer wavelength by a factor of $\sqrt{2}$) shifts the position of the peak and lowers the maximum value by a factor of 2. For $2 \times 10^{-8} I_{\text{sat}}$, the peak fraction of scattered photons was decreased to 2.4%, i.e., by a factor of approximately 3.5. Changing the array separation to 5.02λ shifts the position of the peak and lowers the maximum value by a factor of 4. For $2 \times 10^{-8} I_{\text{sat}}$, the peak fraction of scattered photons decreased to 0.61%, i.e., by another factor of approximately 3.8.

Figure 4 shows the reflection, transmission, and incoherent scattering probabilities versus detuning for two very low intensities. In the weak-field limit on resonance, the reflection probability goes to 0 and the transmission probability goes to 1. As with the one-array case, the biggest change at low intensities is the transfer of transmission probability to incoherently

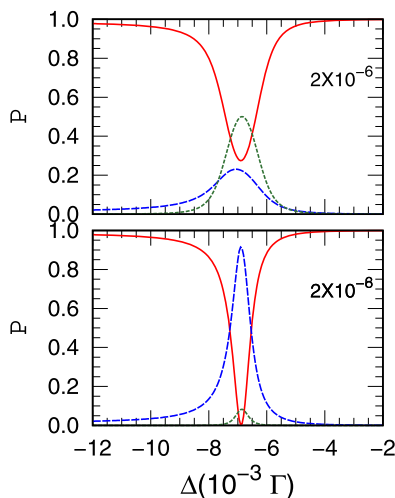


FIG. 4. For a pair of arrays, the reflected (red solid), transmitted (blue dashed), and incoherently scattered (green short dash) probabilities versus detuning for an intensity of 2×10^{-8} and of $2 \times 10^{-6} I_{\text{sat}}$. The array properties are the same as for Fig. 2.

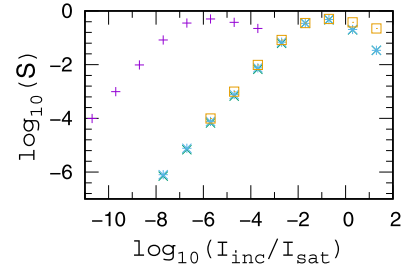


FIG. 5. The maximum incoherent scattering (S) versus incident intensity for two arrays calculated using MF1 (purple +) and for one array calculated using MF2 (green \times) and MF1 (blue $*$). The orange squares are the same as the purple + but with I_{inc} multiplied by 10^5 .

scattered probability. For example, for the $2 \times 10^{-8} I_{\text{sat}}$ case, the reflection probability on resonance is less than 1% while the transmitted probability has decreased to approximately 92%. For the $2 \times 10^{-6} I_{\text{sat}}$ case, the reflection probability on resonance is approximately 28%, which is more than the approximately 23% transmitted. Another clear feature is the increase in resonance width with increasing intensity. Obviously, there is no relevant power broadening for intensity of $2 \times 10^{-6} I_{\text{sat}}$ but the linewidth is clearly much larger than that for the weak-field limit.

Figure 5 shows the maximum incoherent scattering probability versus the incident intensity for one and two arrays. This shows the linear rise of S with intensity for small intensities and then the subsequent decrease as the atom excitation is saturated. It also shows the relatively large amount of scattering for the two-array cavity, which only has an intensity enhancement of a factor of $\simeq 500$. The two-array scattering overlaps the one array for small I_{inc} if the two-array intensity is increased by a factor of $\sim 10^5$. Both the average intensity between the arrays and the scattering probabilities show that even quite weak laser intensity can lead to qualitative changes.

C. Extent of the near field

In our calculations, the main parameters derive from the asymptotic behavior of the light. For example, the reflection, transmission, and incoherent scattering probabilities are all asymptotic properties. Clearly, the light is not a plane wave in the neighborhood of the atoms. So an important question is how the light field becomes a plane wave as a function of distance from an atom array. This is a natural question, because the near field could affect results. For example, we chose the atoms in both arrays to be at the same y, z positions in Sec. VB. This choice is irrelevant if the field has become a plane wave over the distance between the two arrays.

The main dependence of the decay arises from the periodicity in the light fields due to the atom array. Because the atom array repeats after a displacement of $a < \lambda$ in the y or z directions, the light fields must have $(k_y, k_z) = (2\pi/a)(n_y, n_z)$, with n_i being integers. Only for $n_y = n_z = 0$ is the resulting wave number in the x direction real. For other values, the x direction will exponentially decrease with $\kappa_x = k\sqrt{(n_y^2 + n_z^2)(\lambda/a)^2 - 1}$. The slowest decrease will be when

$n_y^2 + n_z^2 = 1$, giving an exponential decrease

$$\text{near field} \sim e^{-\kappa_x x}, \quad (29)$$

with $\kappa_x = k\sqrt{(\lambda/a)^2 - 1}$. For the examples in the figures, we used $a = 0.8\lambda$, giving $\kappa_x = 4.71/\lambda$. Thus, the size of the near field has decreased by a factor of $\sim 6 \times 10^{-11}$ between the two arrays in Sec. VB. We tested this by subtracting the asymptotic form in Eq. (B8) from a numerical summation of the first line and exactly found this exponential decay. This can lead to surprisingly fast decay of the near field when the atom separation is small. For example, for $a = 0.6\lambda$, $\kappa_x = 8.38/\lambda$, giving a near-field decay by a factor of ~ 4000 after only one wavelength.

D. Photon correlations

These studies were partly motivated by the possibility for investigating correlations between photons reflected, scattered, or transmitted through the arrays. There have been several studies for finite arrays—for example, Refs. [18,27,29]. Unfortunately, the infinite array cases do not display interesting behavior with regards to, for example, the $g^{(2)}$ functions for photons. One can show that all combinations of $g^{(2)}$ are equal to 1 for all times because the range of atom correlations is finite but the arrays extend to infinity. Thus, only finite size arrays or focused light beams lead to nontrivial $g^{(2)}$ for the geometry investigated here.

VI. SUMMARY

We have developed a computationally tractable theory for light interacting with infinite atom array(s) beyond the weak-field approximation used in previous investigations. The infinite extent of the arrays provides both a challenge and a simplification to quantitatively understanding the dynamics. We mainly focus on the behavior of the coherently reflected or transmitted photons and the incoherently scattered photons versus the intensity and detuning of the light, with a focus on how larger intensities modify the transmission, reflection, and incoherent scattering properties. Results were presented for both a single-atom array as well as a pair of atom arrays with a separation that leads to cavity enhancement of light between the arrays.

The basic computational tool was the mean-field approximation. Calculations were performed using simple mean field (MF1) as well as a more elaborate mean field (MF2): in MF1, expectation values of products of operators are replaced by products of expectation values, while MF2 replaces expectation values of a triple product by pairwise and single expectation values. One of the main results is the reduction of the infinite number of equations into a finite number that well represents this system. We also give practical methods for evaluating the infinite sums for important parameters.

The basic physical question addressed was how larger intensity modifies the interaction of the array(s) with light. For a single array, we showed that the MF1 and MF2 results were nearly the same except for a small range of intensity. As might be expected, the fraction of incoherently scattered photons increases with increasing Rabi frequency Ω , until the intensity is large enough to begin saturating the transition. At

larger intensity, the coherently reflected and transmitted probabilities are changed in characteristic ways. For example, on resonance, the coherently reflected probability decreases from 1 with increasing intensity while the coherently transmitted probability increases from 0. For the case of two arrays with separation to give cavity enhancement of photons between them, the changes to the transmitted and reflected probabilities are substantial for tiny-incident laser intensities.

Data plotted in the figures is available at Ref. [48].

ACKNOWLEDGMENTS

F.R. thanks Igor Ferrier-Barbut for a discussion that motivated the form of Eqs. (8) and (13). This work was supported by the National Science Foundation under Grant No. 2109987-PHY.

APPENDIX A: TWO-ATOM TERMS

This section gives the terms that arise from the dipole-dipole interaction. In the one-atom equations of motion, there are terms that arise from the interaction between pairs of atoms. Because the single-atom expectation values are independent of atom position, the only important terms are

$$\begin{aligned} \frac{d\langle\hat{\sigma}_0^-\rangle}{dt} &= \sum_{m \neq 0} g_{m0} \langle(2\hat{e}_0 - 1)\hat{\sigma}_m^-\rangle \\ \frac{d\langle\hat{e}_0\rangle}{dt} &= - \sum_{m \neq 0} [g_{m0} \langle\hat{\sigma}_0^+ \hat{\sigma}_m^-\rangle + g_{m0}^* \langle\hat{\sigma}_0^- \hat{\sigma}_m^+\rangle]. \end{aligned} \quad (A1)$$

In the two-atom equations of motion, the dipole-dipole terms in the differential equations are complicated, so we have broken them up into 16 different terms. Only in the first of these, V_1 , will we explicitly show the conversion of the expectation value of triple operators into pairs and singles. Remember, all single-atom expectation values can be replaced as $\langle\hat{e}_n\rangle = \langle\hat{e}_0\rangle$. These terms are

$$\begin{aligned} V_1 &= \sum_{m \neq n, 0} g_{m0} \langle\hat{\sigma}_0^+ \hat{\sigma}_n^- \hat{\sigma}_m^-\rangle \\ &\rightarrow \sum_{m \neq n, 0} g_{m0} (\langle\hat{\sigma}_0^+\rangle \langle\hat{\sigma}_n^- \hat{\sigma}_m^-\rangle + \langle\hat{\sigma}_0^+ \hat{\sigma}_n^-\rangle \langle\hat{\sigma}_m^-\rangle \\ &\quad + \langle\hat{\sigma}_0^+ \hat{\sigma}_m^-\rangle \langle\hat{\sigma}_n^-\rangle - 2\langle\hat{\sigma}_0^+\rangle \langle\hat{\sigma}_n^-\rangle \langle\hat{\sigma}_m^-\rangle) \\ &= (\mathcal{G} - g_{n0}) (\langle\hat{\sigma}_0^+ \hat{\sigma}_n^-\rangle - 2\langle\hat{\sigma}_0^+\rangle \langle\hat{\sigma}_n^-\rangle) \langle\hat{\sigma}_m^-\rangle \\ &\quad + (\mathcal{C}_0^+ - g_{n0} \langle\hat{\sigma}_0^+ \hat{\sigma}_n^-\rangle) \langle\hat{\sigma}_m^-\rangle + \mathcal{C}_n^- \langle\hat{\sigma}_0^+\rangle \end{aligned} \quad (A2)$$

$$\begin{aligned} V_2 &= \sum_{m \neq n, 0} g_{m0}^* \langle\hat{\sigma}_0^- \hat{\sigma}_n^- \hat{\sigma}_m^+\rangle \\ &= (\mathcal{G}^* - g_{n0}^*) (\langle\hat{\sigma}_0^- \hat{\sigma}_n^-\rangle - 2\langle\hat{\sigma}_0^-\rangle \langle\hat{\sigma}_n^-\rangle) \langle\hat{\sigma}_m^+\rangle \\ &\quad + (\mathcal{C}_0^{+*} - g_{n0}^* \langle\hat{\sigma}_0^- \hat{\sigma}_n^-\rangle) \langle\hat{\sigma}_m^+\rangle + \mathcal{C}_n^{+*} \langle\hat{\sigma}_0^-\rangle \end{aligned} \quad (A3)$$

$$\begin{aligned} V_3 &= \sum_{m \neq n, 0} g_{mn} \langle\hat{e}_0 \hat{e}_n \hat{\sigma}_m^-\rangle \\ &= (\mathcal{G} - g_{-n0}) (\langle\hat{e}_0 \hat{e}_{-n}\rangle - 2\langle\hat{e}_0\rangle \langle\hat{e}_n\rangle) \langle\hat{\sigma}_m^-\rangle \\ &\quad + (\mathcal{C}_0^0 - g_{-n0} \langle\hat{e}_0 \hat{e}_{-n}\rangle) \langle\hat{e}_0\rangle + \mathcal{C}_{-n}^0 \langle\hat{e}_n\rangle \end{aligned} \quad (A4)$$

$$V_4 = \sum_{m \neq n, 0} g_{mn} \langle \hat{e}_0 \hat{\sigma}_m^- \rangle = C_{-n}^0 \quad (\text{A5})$$

$$\begin{aligned} V_5 &= \sum_{m \neq n, 0} g_{m0} \langle \hat{e}_0 \hat{\sigma}_n^- \hat{\sigma}_m^- \rangle \\ &= (\mathcal{G} - g_{n0}) (\langle \hat{e}_0 \hat{\sigma}_n^- \rangle - 2 \langle \hat{e}_0 \rangle \langle \hat{\sigma}_0^- \rangle) \langle \hat{\sigma}_0^- \rangle \\ &\quad + (C_0^0 - g_{n0} \langle \hat{e}_0 \hat{\sigma}_n^- \rangle) \langle \hat{\sigma}_0^- \rangle + C_n^- \langle \hat{e}_0 \rangle \end{aligned} \quad (\text{A6})$$

$$V_6 = \sum_{m \neq n, 0} g_{m0} \langle \hat{\sigma}_n^- \hat{\sigma}_m^- \rangle = C_n^- \quad (\text{A7})$$

$$\begin{aligned} V_7 &= \sum_{m \neq n, 0} g_{mn} \langle \hat{\sigma}_0^- \hat{e}_n \hat{\sigma}_m^- \rangle \\ &= (\mathcal{G} - g_{-n0}) (\langle \hat{e}_0 \hat{\sigma}_n^- \rangle - 2 \langle \hat{e}_0 \rangle \langle \hat{\sigma}_0^- \rangle) \langle \hat{\sigma}_0^- \rangle \\ &\quad + (C_0^0 - g_{-n0} \langle \hat{e}_0 \hat{\sigma}_n^- \rangle) \langle \hat{\sigma}_0^- \rangle + C_{-n}^- \langle \hat{e}_0 \rangle \end{aligned} \quad (\text{A8})$$

$$V_8 = \sum_{m \neq n, 0} g_{mn} \langle \hat{\sigma}_0^- \hat{\sigma}_m^- \rangle = C_{-n}^- \quad (\text{A9})$$

$$\begin{aligned} V_9 &= \sum_{m \neq n, 0} g_{m0} \langle \hat{\sigma}_0^+ \hat{e}_n \hat{\sigma}_m^- \rangle \\ &= (\mathcal{G} - g_{n0}) (\langle \hat{\sigma}_0^+ \hat{e}_n \rangle - 2 \langle \hat{\sigma}_0^+ \rangle \langle \hat{e}_0 \rangle) \langle \hat{\sigma}_0^- \rangle \\ &\quad + (C_0^+ - g_{n0} \langle \hat{\sigma}_0^+ \hat{\sigma}_n^- \rangle) \langle \hat{e}_0 \rangle + C_n^0 \langle \hat{\sigma}_0^+ \rangle \end{aligned} \quad (\text{A10})$$

$$V_{10} = \sum_{m \neq n, 0} g_{m0}^* \langle \hat{\sigma}_0^+ \hat{e}_n \hat{\sigma}_m^+ \rangle = V_9^* \quad (\text{A11})$$

$$\begin{aligned} V_{11} &= \sum_{m \neq n, 0} g_{mn} \langle \hat{e}_0 \hat{\sigma}_n^+ \hat{\sigma}_m^- \rangle \\ &= (\mathcal{G} - g_{-n0}) (\langle \hat{\sigma}_0^+ \hat{e}_n \rangle - 2 \langle \hat{\sigma}_0^+ \rangle \langle \hat{e}_0 \rangle) \langle \hat{\sigma}_0^- \rangle \\ &\quad + (C_0^+ - g_{-n0} \langle \hat{\sigma}_0^+ \hat{\sigma}_n^- \rangle) \langle \hat{e}_0 \rangle + C_{-n}^0 \langle \hat{\sigma}_0^+ \rangle \end{aligned} \quad (\text{A12})$$

$$V_{12} = \sum_{m \neq n, 0} g_{mn}^* \langle \hat{e}_0 \hat{\sigma}_n^- \hat{\sigma}_m^+ \rangle = V_{11}^* \quad (\text{A13})$$

$$\begin{aligned} V_{13} &= \sum_{m \neq n, 0} g_{m0} \langle \hat{e}_0 \hat{\sigma}_n^+ \hat{\sigma}_m^- \rangle \\ &= (\mathcal{G} - g_{n0}) (\langle \hat{e}_0 \hat{\sigma}_n^+ \rangle - 2 \langle \hat{e}_0 \rangle \langle \hat{\sigma}_0^+ \rangle) \langle \hat{\sigma}_0^- \rangle \\ &\quad + (C_0^0 - g_{n0} \langle \hat{e}_0 \hat{\sigma}_n^+ \rangle) \langle \hat{\sigma}_0^+ \rangle + C_n^+ \langle \hat{e}_0 \rangle \end{aligned} \quad (\text{A14})$$

$$V_{14} = \sum_{m \neq n, 0} g_{m0} \langle \hat{\sigma}_n^+ \hat{\sigma}_m^- \rangle = C_n^+ \quad (\text{A15})$$

$$\begin{aligned} V_{15} &= \sum_{m \neq n, 0} g_{mn}^* \langle \hat{\sigma}_0^- \hat{e}_n \hat{\sigma}_m^+ \rangle \\ &= (\mathcal{G} - g_{-n0})^* (\langle \hat{e}_0 \hat{\sigma}_n^- \rangle - 2 \langle \hat{e}_0 \rangle \langle \hat{\sigma}_0^- \rangle) \langle \hat{\sigma}_0^+ \rangle \\ &\quad + (C_0^0 - g_{-n0} \langle \hat{e}_0 \hat{\sigma}_n^- \rangle)^* \langle \hat{\sigma}_0^- \rangle + C_{-n}^{+*} \langle \hat{e}_0 \rangle \end{aligned} \quad (\text{A16})$$

$$V_{16} = \sum_{m \neq n, 0} g_{mn}^* \langle \hat{\sigma}_0^- \hat{\sigma}_m^+ \rangle = C_{-n}^{+*}, \quad (\text{A17})$$

used in these equations are

$$C_n^\pm = \sum_{m \neq 0, n} g_{m0} \langle \hat{\sigma}_n^\pm \hat{\sigma}_m^- \rangle \quad (\text{A18})$$

$$C_n^0 = \sum_{m \neq 0, n} g_{m0} \langle \hat{e}_n \hat{\sigma}_m^- \rangle. \quad (\text{A19})$$

We discuss the numerical evaluations of these three parameters in Appendix C.

APPENDIX B: QUANTUM LIGHT INTENSITY

This section gives the equations for how to calculate the light intensity in the presence of the atom array(s). The flux of photons will be given in terms of the expectation values of the atom operators. Some care is needed to ensure the infinite sums are handled correctly. The derivation is for a plane wave normally incident on the atom array and will compute the relative photon flux at a large distance from the arrays.

Following Ref. [19], we start from the field operators

$$\eta_E^+(\mathbf{r}) = \hat{\varepsilon} e^{i\mathbf{k} \cdot \mathbf{r}} - \frac{2i}{\Omega} \sum_n \mathbf{g}_E(\mathbf{r}_n) \hat{\sigma}_n^- \quad (\text{B1})$$

$$\eta_B^+(\mathbf{r}) = \hat{k} \times \hat{\varepsilon} e^{i\mathbf{k} \cdot \mathbf{r}} - \frac{2i}{\Omega} \sum_n \mathbf{g}_B(\mathbf{r}_n) \hat{\sigma}_n^- \quad (\text{B2})$$

$$\mathbf{g}_E(\mathbf{R}) = \frac{3\Gamma}{4} \frac{e^{i\mathbf{k} \cdot \mathbf{R}}}{ikR} [\hat{\varepsilon} - (\hat{\varepsilon} \cdot \hat{R}) \hat{R}] \quad (\text{B3})$$

$$\mathbf{g}_B(\mathbf{R}) = \hat{R} \times \mathbf{g}_E(\mathbf{R}), \quad (\text{B4})$$

with $\mathbf{r}_n = \mathbf{r} - \mathbf{R}_n$, $\hat{\varepsilon}$ being the unit vector for the laser polarization and the dipole of the atom, and $r_n \gg \lambda$. Because of the last condition, the asymptotic, $|\mathbf{R}| \rightarrow \infty$, form of the electric- and magnetic-field amplitudes, $\mathbf{g}_{E,B}(\mathbf{R})$, are used. The field operators have been scaled by a factor proportional to the Rabi frequency so that the coherent reflection, coherent transmission, and incoherent scattered probabilities are easily obtained. For all of the calculations in this paper, the $\vec{r} = x\hat{k}$ with $x \rightarrow \pm\infty$, i.e., the evaluation of the fields will be at a large distance from the array above or below the origin. The relative flux of photons in the direction \hat{k} is

$$\mathcal{F}(\mathbf{r}) = \frac{1}{2} \hat{k} \cdot \langle \eta_E^- \times \eta_B^+ - \eta_B^- \times \eta_E^+ \rangle. \quad (\text{B5})$$

To evaluate the expression, it is simplest to use the classical expression and the difference from the classical value:

$$\mathcal{F}(\mathbf{r}) = \mathcal{F}_{cl}(\mathbf{r}) + \mathcal{S}(\mathbf{r}), \quad (\text{B6})$$

with $\mathcal{F}_{cl}(\mathbf{r})$ the classical value, which is coherent with the driving laser, and $\mathcal{S}(\mathbf{r})$, which is incoherent and describes the scattered photons.

The classical expression is

$$\mathcal{F}_{cl}(\mathbf{r}) = \frac{1}{2} \hat{k} \cdot (\langle \eta_E^- \rangle \times \langle \eta_B^+ \rangle - \langle \eta_B^- \rangle \times \langle \eta_E^+ \rangle), \quad (\text{B7})$$

where the large-distance expressions can be found analytically. For a single array, the classical field is

$$\langle \eta_E^+ \rangle = \hat{\varepsilon} e^{i\mathbf{k} \cdot \mathbf{r}} - \frac{2i}{\Omega} \langle \hat{\sigma}^- \rangle \sum_n \mathbf{g}_E(\mathbf{r}_n) \rightarrow \hat{\varepsilon} (e^{i\mathbf{k} \cdot \mathbf{r}} + \mathcal{R} e^{i\mathbf{k} \cdot |\mathbf{r}|}), \quad (\text{B8})$$

where the \mathcal{G} is defined in Eq. (7) and subscript $-n$ means the atom identified by the point $-n_y, -n_z$. The other parameters

with the reflection amplitude \mathcal{R} given by

$$\mathcal{R} = -\frac{3i\Gamma\pi}{\Omega k^2 a^2} \langle \hat{\sigma}^- \rangle \quad (\text{B9})$$

because $|x| \gg a$. This result was found using the relation $d_n^2 = x^2 + y_n^2 + z_n^2$ to get

$$\begin{aligned} \sum_n \frac{e^{ikd_n}}{ikd_n} \left(1 - \frac{z_n^2}{d_n^2}\right) &\rightarrow \frac{1}{ia^2} \iint \frac{e^{ikd}}{kd} \left(1 - \frac{z^2}{d^2}\right) dydz \\ &= \frac{2\pi}{k^2 a^2} e^{ik|x|} \end{aligned} \quad (\text{B10})$$

for $|x| \gg a$. This expression is for linear polarization *and* for circular polarization because replacing z_n^2 with $(1/2)(y_n^2 + z_n^2)$ leads to the same result. For a pair of arrays, the classical field is

$$\langle \eta_E^+ \rangle \rightarrow \hat{\varepsilon} (e^{ikx} + \mathcal{R}_\alpha e^{ik|x|} + \mathcal{R}_\beta e^{ik|x-L|}), \quad (\text{B11})$$

as $|x| \gg a$, with the subscript on \mathcal{R} indicating which expectation value is used in Eq. (B9).

The scattering terms arise from the cumulant of the pairwise expectation values ($\langle \hat{A}\hat{B} \rangle - \langle \hat{A} \rangle \langle \hat{B} \rangle$) in Eq. (B6):

$$S(\mathbf{r}) = \mathcal{Q}^{(1)}(\mathbf{r}) + \mathcal{Q}^{(2)}(\mathbf{r}), \quad (\text{B12})$$

where the $\mathcal{Q}^{(1)}$ and $\mathcal{Q}^{(2)}$ are derived separately. As $|x| \rightarrow \infty$, the $\mathcal{Q}^{(1)}$ and $\mathcal{Q}^{(2)}$ each go to a constant because there cannot be phase information from the incoherent scattering from all of the atoms in the array.

The one-atom terms arise because $\hat{\sigma}_n^+ \hat{\sigma}_n^- = \hat{e}_n$ converts a two-operator expectation value to a single-operator expectation value. This term is

$$\begin{aligned} \mathcal{Q}^{(1)} &= \left(\frac{3\Gamma}{2k\Omega}\right)^2 [\langle \hat{e} \rangle - |\langle \hat{\sigma}^+ \rangle|^2] \sum_n \langle \hat{k} \cdot \hat{r}_n \rangle \frac{1 - |\hat{\varepsilon} \cdot \hat{r}_n|^2}{r_n^2} \\ &\rightarrow 3\pi \left(\frac{\Gamma}{\Omega ka}\right)^2 [\langle \hat{e} \rangle - |\langle \hat{\sigma}^+ \rangle|^2], \end{aligned} \quad (\text{B13})$$

where $\vec{r}_n = \mathbf{r} - \mathbf{R}_n$ with $x \rightarrow \pm\infty$. This result was found using the relation $d_n^2 = x^2 + y_n^2 + z_n^2$ to get

$$\begin{aligned} \sum_n \frac{|x|}{d_n^3} \left(1 - \frac{z_n^2}{d_n^2}\right) &\rightarrow \frac{1}{a^2} \iint \frac{|x|}{d^3} \left(1 - \frac{z^2}{d^2}\right) dydz \\ &= \frac{4\pi}{3a^2} \end{aligned} \quad (\text{B14})$$

in the limit $|x| \rightarrow \infty$. This expression is the same for linear or circular polarization. Note that $\mathcal{Q}^{(1)}$ is the same in the $+x$ or $-x$ directions, so the calculation of the total incoherent scattering probability needs to double these values.

The two-atom terms must have the form

$$\mathcal{Q}^{(2)} \rightarrow \sum_{m \neq 0} q_m [\langle \hat{\sigma}_0^+ \hat{\sigma}_m^- \rangle - \langle \hat{\sigma}_0^+ \rangle \langle \hat{\sigma}_m^- \rangle], \quad (\text{B15})$$

with q_m independent of position. For linear polarization,

$$q_m \rightarrow \left(\frac{3\Gamma}{2\Omega k}\right)^2 \sum_n \frac{|x|}{d_n^3} \left(1 - \frac{z_n^2}{d_n^2}\right) e^{ik(n_y m_y + n_z m_z) a^2 / d_n} \quad (\text{B16})$$

in the limit $|x| \rightarrow \infty$. We have not found a simple closed-form solution for this expression. For example, the q_m can

be written in terms of integrals over J_0, J_2 cylindrical Bessel functions or as a series in powers of $k^2 a^2 (m_y^2 + m_z^2)$. Unfortunately, the series has difficulty with round-off errors as $k^2 a^2 (m_y^2 + m_z^2)$ becomes large, so we only used the integral over Bessel functions:

$$q_m \rightarrow \pi \left(\frac{3\Gamma}{2\Omega ka}\right)^2 \int_0^\infty \frac{\rho |x|}{(x^2 + \rho^2)^{3/2}} \left\{ \frac{2x^2 + \rho^2}{x^2 + \rho^2} J_0[s(\rho)] - \frac{\rho^2}{x^2 + \rho^2} \frac{m_y^2 - m_z^2}{m_y^2 + m_z^2} J_2[s(\rho)] \right\} d\rho \quad (\text{B17})$$

$$s(\rho) = ka \frac{\rho}{\sqrt{x^2 + \rho^2}} \sqrt{m_y^2 + m_z^2}, \quad (\text{B18})$$

where the integration was done numerically. For large $|x|$, the q_m is independent of x . For circular polarization, the only change is to drop the term with $J_2(s)$ because then the q_m can only depend on $m_y^2 + m_z^2$.

APPENDIX C: NUMERICAL METHODS

While the various summations of parameters converge, their numerical evaluation can be difficult if used in their simple form. In this section, we give the numerical methods we used to evaluate various expressions.

The summation for \mathcal{G} only slowly converges with system size. For example, writing

$$\mathcal{G}(N) = \sum_{m \neq 0}^{m_y^2 + m_z^2 < N^2} g(\mathbf{R}_m) \quad (\text{C1})$$

$$\mathcal{G} = \lim_{N \rightarrow \infty} \mathcal{G}(N) \quad (\text{C2})$$

only slowly converges because it is similar to integrating $\exp[ik\rho]/\rho$ in cylindrical coordinates. Thus, the hard limit to the summation gives an effect similar to Gibbs phenomenon where the $\mathcal{G}(N)$ oscillates around the limit. Instead, we used a function to smoothly cut off the sum

$$\mathcal{G}(N) = \sum_{m \neq 0}^{m_y^2 + m_z^2 < N^2} g(\mathbf{R}_m) e^{-36(m_y^2 + m_z^2)^2 / N^4}, \quad (\text{C3})$$

with \mathcal{G} being the limit as $N \rightarrow \infty$. As we increased N , this expression smoothly approaches \mathcal{G} so that the numerical calculation is unambiguous. As a test, we compare the real part of $\mathcal{G}(N)$ to $(\Gamma/2)\{(3/[4\pi]) (\lambda/a)^2 - 1\}$. For example, for $a = 0.8\lambda$, the fractional error from Eq. (C3) of the real part of \mathcal{G} was 1.1×10^{-9} for $N = 125$, 6.9×10^{-11} for 250, 4.3×10^{-12} for 500, 2.7×10^{-13} for 1000, and 1.8×10^{-14} for 1500, whereas Eq. (C1) gives fractional errors of 0.080 for $N = 125$, 0.056 for 250, 0.040 for 500, 0.028 for 1000, and 0.023 for 1500.

For similar reasons, the summation for $\bar{\mathcal{G}}$ used in the two-array calculations does not converge well with system size. We use the same kind of smooth cutoff

$$\bar{\mathcal{G}}(N) = e^{-ikL} \sum_{m_\beta}^{m_y^2 + m_z^2 < N^2} g(\mathbf{R}_{m_\beta}) e^{-36(m_y^2 + m_z^2)^2 / N^4}, \quad (\text{C4})$$

where $\mathbf{R}_{m_\beta} = (L, m_y a, m_z a)$ and $\bar{\mathcal{G}}$ is the limit as $N \rightarrow \infty$. Because of the L in the position, the N has to be much larger

than L/a , which sometimes means using more terms than needed to converge \mathcal{G} . But as before, this expression smoothly converges with N , giving an unambiguous value for smaller computational cost. When $L \gg \lambda$, the summation can be done analytically using the same expression in Eq. (B10) multiplied by $3\Gamma/4$ and $\exp(-ikL)$, which gives

$$\bar{\mathcal{G}} \rightarrow \frac{3\pi\Gamma}{2k^2 a^a} \quad \text{for} \quad L \gg \lambda. \quad (\text{C5})$$

In principle, the calculation of $\mathcal{Q}^{(2)}$, Eq. (B15), does not need any convergence help because both the q_m and the cumulant decrease with increasing $m_y^2 + m_z^2$. In practice, the results converge faster with a similar, smooth cutoff function. For MF2, the calculation extends over terms with $\sqrt{m_y^2 + m_z^2} \leq N_w$. In our calculations, we did calculations with $N_w = 15, 20, 25,$

and 30. The calculation of $\mathcal{Q}^{(2)}$ converged faster when we used

$$\mathcal{Q}^{(2)} = \sum_{m \neq 0}^{m_y^2 + m_z^2 < N_w^2} q_m [\langle \hat{\sigma}_0^+ \hat{\sigma}_m^- \rangle - \langle \hat{\sigma}_0^+ \rangle \langle \hat{\sigma}_0^- \rangle] W_m \quad (\text{C6})$$

with

$$W_m = e^{-36(m_y^2 + m_z^2)^2 / N_w^4}. \quad (\text{C7})$$

As with \mathcal{G} , the weight function causes a smooth cutoff of the cumulants times an oscillating term, leading to faster convergence.

The calculation of the $\mathcal{C}_n^{\pm,0}$ parameters in the two-atom equations in Appendix A converge in a similar way to the \mathcal{G} parameters. However, we do not have the luxury of using the same type of smooth cutoff because the $\mathcal{C}_n^{\pm,0}$ contains expectation values of pair operators, neither at the origin. For these parameters, we used the sum as written.

-
- [1] D. E. Chang, J. Ye, and M. D. Lukin, Controlling dipole-dipole frequency shifts in a lattice-based optical atomic clock, *Phys. Rev. A* **69**, 023810 (2004).
- [2] Z. Meir, O. Schwartz, E. Shahmoon, D. Oron, and R. Ozeri, Cooperative Lamb Shift in a Mesoscopic Atomic Array, *Phys. Rev. Lett.* **113**, 193002 (2014).
- [3] S. D. Jenkins and J. Ruostekoski, Controlled manipulation of light by cooperative response of atoms in an optical lattice, *Phys. Rev. A* **86**, 031602(R) (2012).
- [4] R. J. Bettles, S. A. Gardiner, and C. S. Adams, Enhanced Optical Cross Section via Collective Coupling of Atomic Dipoles in a 2D Array, *Phys. Rev. Lett.* **116**, 103602 (2016).
- [5] R. T. Sutherland and F. Robicheaux, Collective dipole-dipole interactions in an atomic array, *Phys. Rev. A* **94**, 013847 (2016).
- [6] G. Facchinetti, S. D. Jenkins, and J. Ruostekoski, Storing Light with Subradiant Correlations in Arrays of Atoms, *Phys. Rev. Lett.* **117**, 243601 (2016).
- [7] E. Shahmoon, D. S. Wild, M. D. Lukin, and S. F. Yelin, Cooperative Resonances in Light Scattering from Two-Dimensional Atomic Arrays, *Phys. Rev. Lett.* **118**, 113601 (2017).
- [8] A. Grankin, P.-O. Guimond, D. V. Vasilyev, B. Vermersch, and P. Zoller, Free-space photonic quantum link and chiral quantum optics, *Phys. Rev. A* **98**, 043825 (2018).
- [9] D. E. Chang, J. S. Douglas, A. González-Tudela, C.-L. Hung, and H. J. Kimble, Colloquium: Quantum matter built from nanoscopic lattices of atoms and photons, *Rev. Mod. Phys.* **90**, 031002 (2018).
- [10] A. Asenjo-Garcia, M. Moreno-Cardoner, A. Albrecht, H. J. Kimble, and D. E. Chang, Exponential Improvement in Photon Storage Fidelities Using Subradiance and “Selective Radiance” in Atomic Arrays, *Phys. Rev. X* **7**, 031024 (2017).
- [11] A. Asenjo-Garcia, H. J. Kimble, and D. E. Chang, Optical waveguiding by atomic entanglement in multilevel atom arrays, *Proc. Natl. Acad. Sci. USA* **116**, 25503 (2019).
- [12] L. Henriët, J. S. Douglas, D. E. Chang, and A. Albrecht, Critical open-system dynamics in a one-dimensional optical-lattice clock, *Phys. Rev. A* **99**, 023802 (2019).
- [13] J. A. Needham, I. Lesanovsky, and B. Olmos, Subradiance-protected excitation transport, *New J. Phys.* **21**, 073061 (2019).
- [14] C. Qu and A. M. Rey, Spin squeezing and many-body dipolar dynamics in optical lattice clocks, *Phys. Rev. A* **100**, 041602 (2019).
- [15] Y.-X. Zhang and K. Mølmer, Theory of Subradiant States of a One-Dimensional Two-Level Atom Chain, *Phys. Rev. Lett.* **122**, 203605 (2019).
- [16] S. J. Masson, I. Ferrier-Barbut, L. A. Orozco, A. Browaeys, and A. Asenjo-Garcia, Many-Body Signatures of Collective Decay in Atomic Chains, *Phys. Rev. Lett.* **125**, 263601 (2020).
- [17] J. Javanainen and R. Rajapakse, Light propagation in systems involving two-dimensional atomic lattices, *Phys. Rev. A* **100**, 013616 (2019).
- [18] L. A. Williamson, M. O. Borgh, and J. Ruostekoski, Superatom Picture of Collective Nonclassical Light Emission and Dipole Blockade in Atom Arrays, *Phys. Rev. Lett.* **125**, 073602 (2020).
- [19] L. A. Williamson and J. Ruostekoski, Optical response of atom chains beyond the limit of low light intensity: The validity of the linear classical oscillator model, *Phys. Rev. Res.* **2**, 023273 (2020).
- [20] R. J. Bettles, M. D. Lee, S. A. Gardiner, and J. Ruostekoski, Quantum and nonlinear effects in light transmitted through planar atomic arrays, *Commun. Phys.* **3**, 141 (2020).
- [21] P.-O. Guimond, A. Grankin, D. V. Vasilyev, B. Vermersch, and P. Zoller, Subradiant Bell States in Distant Atomic Arrays, *Phys. Rev. Lett.* **122**, 093601 (2019).
- [22] K. E. Ballantine and J. Ruostekoski, Optical Magnetism and Huygens’ Surfaces in Arrays of Atoms Induced by Cooperative Responses, *Phys. Rev. Lett.* **125**, 143604 (2020).
- [23] R. Bekenstein, I. Pikovski, H. Pichler, E. Shahmoon, S. F. Yelin, and M. D. Lukin, Quantum metasurfaces with atom arrays, *Nat. Phys.* **16**, 676 (2020).
- [24] J. Rui, D. Wei, A. Rubio-Abadal, S. Hollerith, J. Zeiher, D. M. Stamper-Kurn, C. Gross, and I. Bloch, A subradiant optical mirror formed by a single structured atomic layer, *Nature (London)* **583**, 369 (2020).
- [25] A. Cidrim, T. S. do Espirito Santo, J. Schachenmayer, R. Kaiser, and R. Bachelard, Photon Blockade with Ground-State Neutral Atoms, *Phys. Rev. Lett.* **125**, 073601 (2020).

- [26] K. E. Ballantine and J. Ruostekoski, Cooperative optical wavefront engineering with atomic arrays, *Nanophotonics* **10**, 1901 (2021).
- [27] D. Cano, Photon statistics of the light transmitted and reflected by a two-dimensional atomic array, *Phys. Rev. A* **104**, 053709 (2021).
- [28] K. E. Ballantine and J. Ruostekoski, Unidirectional absorption, storage, and emission of single photons in a collectively responding bilayer atomic array, *Phys. Rev. Res.* **4**, 033200 (2022).
- [29] S. P. Pedersen, L. Zhang, and T. Pohl, Quantum nonlinear metasurfaces from dual arrays of ultracold atoms, *Phys. Rev. Res.* **5**, L012047 (2023).
- [30] T. L. Patti, D. S. Wild, E. Shahmoon, M. D. Lukin, and S. F. Yelin, Controlling Interactions between Quantum Emitters Using Atom Arrays, *Phys. Rev. Lett.* **126**, 223602 (2021).
- [31] F. Robicheaux, Theoretical study of early-time superradiance for atom clouds and arrays, *Phys. Rev. A* **104**, 063706 (2021).
- [32] O. Rubies-Bigorda and S. F. Yelin, Superradiance and subradiance in inverted atomic arrays, *Phys. Rev. A* **106**, 053717 (2022).
- [33] S. J. Masson and A. Asenjo-Garcia, Universality of Dicke superradiance in arrays of quantum emitters, *Nat. Commun.* **13**, 2285 (2022).
- [34] E. Sierra, S. J. Masson, and A. Asenjo-Garcia, Dicke superradiance in ordered lattices: Dimensionality matters, *Phys. Rev. Res.* **4**, 023207 (2022).
- [35] O. Rubies-Bigorda, S. Ostermann, and S. F. Yelin, Characterizing superradiant dynamics in atomic arrays via a cumulant expansion approach, *Phys. Rev. Res.* **5**, 013091 (2023).
- [36] O. Rubies-Bigorda, S. Ostermann, and S. F. Yelin, Generating multi-excitation subradiant states in incoherently excited atomic arrays, *Phys. Rev. A* **107**, L051701 (2023).
- [37] F. Robicheaux and D. A. Suresh, Beyond lowest order mean-field theory for light interacting with atom arrays, *Phys. Rev. A* **104**, 023702 (2021).
- [38] R. Kubo, Generalized cumulant expansion method, *J. Phys. Soc. Jpn.* **17**, 1100 (1962).
- [39] M. Fleischhauer and S. F. Yelin, Radiative atom-atom interactions in optically dense media: Quantum corrections to the Lorentz-Lorenz formula, *Phys. Rev. A* **59**, 2427 (1999).
- [40] G.-D. Lin and S. F. Yelin, Superradiance in spin- j particles: Effects of multiple levels, *Phys. Rev. A* **85**, 033831 (2012).
- [41] S. Krämer and H. Ritsch, Generalized mean-field approach to simulate the dynamics of large open spin ensembles with long range interactions, *Eur. Phys. J. D* **69**, 282 (2015).
- [42] P. Kirton and J. Keeling, Superradiant and lasing states in driven-dissipative Dicke models, *New J. Phys.* **20**, 015009 (2018).
- [43] P. Kirton, M. M. Roses, J. Keeling, and E. G. Dalla Torre, Introduction to the Dicke model: From equilibrium to nonequilibrium, and vice versa, *Adv. Quantum Technol.* **2**, 1800043 (2019).
- [44] L. Ostermann, C. Meignant, C. Genes, and H. Ritsch, Super- and subradiance of clock atoms in multimode optical waveguides, *New J. Phys.* **21**, 025004 (2019).
- [45] C. Hotter, D. Plankensteiner, and H. Ritsch, Continuous narrowband lasing with coherently driven V-level atoms, *New J. Phys.* **22**, 113021 (2020).
- [46] M. Sánchez-Barquilla, R. E. F. Silva, and J. Feist, Cumulant expansion for the treatment of light-matter interactions in arbitrary material structures, *J. Chem. Phys.* **152**, 034108 (2020).
- [47] J. D. Jackson, *Classical Electrodynamics*, 3rd ed. (John Wiley, New York, 1999).
- [48] Data for: Intensity effects of light coupling to one- or two-atom arrays of infinite extent, <https://doi.org/10.4231/NWKJ-4B32>.